

Monitored Distillation for Positive Congruent Depth Completion

Tian Yu Liu¹, Parth Agrawal¹, Allison Chen¹,
Byung-Woo Hong², and Alex Wong³

¹ UCLA Vision Lab, Los Angeles, CA 90095, USA
{[tianyu139](mailto:tianyu139@ucla.edu),[parthagraawal24](mailto:parthagraawal24@ucla.edu),[allisonchen2](mailto:allisonchen2@ucla.edu)}@g.ucla.edu

² Chung-Ang University, Heukseok-Dong, Dongjak-Gu, Seoul, 06973, Korea
hong@cau.ac.kr

³ UCLA Vision Lab, Los Angeles, CA 90095, USA
alexw@cs.ucla.edu

Abstract. We propose a method to infer a dense depth map from a single image, its calibration, and the associated sparse point cloud. In order to leverage existing models that produce putative depth maps (teacher models), we propose an adaptive knowledge distillation approach that yields a positive congruent training process, where a student model avoids learning the error modes of the teachers. We consider the scenario of a blind ensemble where we do not have access to ground truth for model selection nor training. The crux of our method, termed Monitored Distillation, lies in a validation criterion that allows us to learn from teachers by choosing predictions that best minimize the photometric reprojection error for a given image. The result of which is a distilled depth map and a confidence map, or “monitor”, for how well a prediction from a particular teacher fits the observed image. The monitor adaptively weights the distilled depth where, if all of the teachers exhibit high residuals, the standard unsupervised image reconstruction loss takes over as the supervisory signal. On indoor scenes (VOID), we outperform blind ensembling baselines by 13.3% and unsupervised methods by 20.3%; we boast a 79% model size reduction while maintaining comparable performance to the best supervised method. For outdoors (KITTI), we tie for 5th overall on the benchmark despite not using ground truth.

1 Introduction

Interaction with physical space requires a representation of the 3-dimensional (3D) geometry of the surrounding environment. Most mobile platforms include at least one camera and some means of estimating range at a sparse set of points i.e. a point cloud. These could be from a dedicated range sensor such as a Lidar or radar, or by processing the images using a visual odometry module. Depth completion consists of inferring a dense depth map, with a range value corresponding to every pixel, from an image and a sparse point cloud. Inherently, depth completion is an ill-posed inverse problem, so priors need to be imposed in the form of generic regularization or learned inductive biases.

Natural scenes exhibit regularities that can be captured by a trained model, for instance a deep neural network (DNN), using a dataset of images and corresponding sparse depths. While we wish to avoid any form of manual or ground truth supervision, we also strive to exploit the availability of differing types of pretrained models, whether from synthetic data or other supervised or unsupervised method. We refer to these pretrained models as “teachers,” each providing an hypothesis of depth map for a given image and sparse point cloud. This leads to a blind ensemble setting where ground truth is not available (e.g. transferring models trained on a specific task to new datasets with no ground truth) for the explicit evaluation of pretrained models i.e. model selection. The key question, then, is how to make use of a heterogeneous collection of teachers, along with other variational principles such as minimization of the photometric reprojection error and generic regularizers such as structural similarity.

In general, different teachers will behave differently not only across images, but even across regions within a given image. The incongruency of different models trained on the same tasks has been observed in the context of classification model versioning [57]. Particularly, the same architecture trained with the same data, but starting from different initial conditions can yield models that *differ on a significant portion of the samples* while achieving the same average error rate. Thus, a naive ensembling of a handful of teachers yields the union of the failure modes, only modestly mitigated by the averaging.

Instead, we propose Monitored Distillation for selecting which teacher to emulate in each image at each pixel. The selection is guided by a “monitor”, based on the residual structural similarity between an observed image and its reconstructions generated by each teacher. This yields a spatially-varying confidence map that weights the contribution of the selected teacher as well as the structural and photometric reprojection errors i.e. unsupervised losses, customary in structure-from-motion. In doing so, our method is robust even when poor performing teachers are introduced into the ensemble – discarding their hypotheses in favor of the ones that better reconstruct the scene. In the extreme case where every teacher produces erroneous outputs, our method would still learn a valid depth estimate because of our unsupervised fall-back loss.

Our contributions are as follows: **(i)** We propose an adaptive method to combine the predictions of a blind ensemble of teachers based on the compatibility of their predictions with an observed image; to the best of our knowledge, we are the first to propose knowledge distillation from a blind ensemble for depth completion. **(ii)** The adaptive mechanism yields a spatially varying confidence map or “monitor” that modulates the contributions of each teacher based on their residuals, leading to a training method that is positive congruent. **(iii)** Even when all members of the ensemble fails, our model automatically reverts to the unsupervised learning criteria and generic regularization, allowing us to avoid distilling erroneous knowledge from teachers. **(iv)** Our method outperforms distillation and unsupervised methods by 13.3% and 20.3% respectively on indoors scenes; we are comparable to top supervised methods with a 79%

model size reduction. On the KITTI benchmark, we tie for 5th overall despite not using ground truth.

2 Related Works

Supervised depth completion seeks to regress per-pixel depth values and is trained by minimizing loss with respect to ground truth. Early methods posed the task as learning morphological operators [10] and compressive sensing [8]. Recent works focus on network operations [12,21] and model design [5,35,46,58] to effectively deal with the sparse inputs. For example, [30] used a cascade hour-glass network, [23,58] fused the representations after processing through separate encoders, and [21] proposed an upsampling layer and joint concatenation and convolution. Whereas, [11,12,41,42] learned uncertainty of estimates, [47] leveraged confidence maps to fuse predictions from different modalities, and [40,56,59] used surface normals for guidance. [6,37] use convolutional spatial propagation networks, [20] learned a separate depth and color network and fused them with spatial propagation. While supervised methods currently hold the top ranks on benchmark datasets i.e. KITTI [46] and VOID [53], they inevitably require expensive ground truth for supervision, which is typically unavailable. Furthermore, these architectures are often complex and require many parameters (e.g. 132M for [20], 53.4M for [40] and 25.8M for [37]), hence can be computationally prohibitive to train and impractical to deploy.

Unsupervised depth completion assumes that additional data (stereo or temporally adjacent frames) is available during training. Both stereo [44,58] and monocular [35,51,52,53] paradigms learn to infer dense depth by minimizing (i) the photometric error between the input image and its reconstructions from other views, and (ii) the difference between the prediction and sparse depth input (sparse depth reconstruction). [35] used Perspective-n-Point [29] and RANSAC [14] to align consecutive frames, but is limited in indoor settings. [54] proposed a calibrated backprojection network. However, all of these methods rely on *generic* regularization i.e. local smoothness that is not informed by the data. Attempts to leverage learned priors mainly focused on synthetic data. [34] applied image translation to obtain ground truth in the real domain; whereas [53,58] used synthetic data to learn a prior on the shapes populating a scene. Our method also employs the unsupervised loss, but unlike them, we distill regularization from a blind ensemble of pretrained models, which can be trained on synthetic or real data, supervised or unsupervised.

Knowledge Distillation uses a simpler student model to approximate the function learned by a larger, more complex teacher model by training it to learn the soft target distribution [17]. There exists many works on knowledge distillation, including image classification [33,43,55], object detection [2,3,4], semantic segmentation [31,36,38], depth estimation [19,32,49], and more recently, depth completion [22]. [9,31,32] utilize pairwise and holistic distillation to capture structural relationships and [36] distills latent representations to guide learning. [49] leverages knowledge distillation for monocular depth estimation on mobile

devices, and [39] uses cyclic inconsistency and knowledge distillation for unsupervised depth estimation, where the student network is a sub-network of the teacher. In depth completion, [22] uses knowledge distillation for joint training of both teacher and student models. Unlike ours, this method uses ground truth.

Ensemble learning addresses the limitations of a single teacher by distilling information from multiple teachers [15]. If done effectively, the student will learn to extract the most relevant information from each teacher. This has been explored in classification [25,28,48], but fewer works utilize it in dense prediction tasks. [1] uses it for domain adaptation in semantic segmentation and [16] in selecting lidar points for depth completion. We further assume the blind ensemble setting [45] where we lack ground truth for evaluation of the ensemble.

Positive congruent training [57] observed sample-wise inconsistencies in classification versioning, where new models wrongly predict for samples that were previously classified correctly by an older, reference model on the same task and dataset. [57] proposed a framework for positive-congruent training to reduce error rates and inconsistencies by increasing weights of correctly classified samples. They further investigated an ensemble learning based reference model and proposed a classification framework to learn only from correct teacher predictions and ground truth otherwise. Our monitored distillation framework is inspired by positive-congruence, and similarly adapts based on the prediction confidence of each teacher in the ensemble.

3 Method Formulation

We wish to recover the 3D scene from a calibrated RGB image $I : \Omega \subset \mathbb{R}^2 \mapsto \mathbb{R}_+^3$ and its associated sparse depth map projected onto the image plane $z : \Omega_z \subset \Omega \mapsto \mathbb{R}_+$. To do so, we propose learning a function f_θ that takes as input I, z and camera intrinsics K and outputs a dense depth map $\hat{d} := f_\theta(I, z, K) \in \mathbb{R}_+^{H \times W}$.

We assume that for each synchronized pair of image and sparse depth map (I_t, z_t) captured at a viewpoint t , we have access to a set of spatially and/or temporally adjacent alternate views T and the corresponding set of images I_T . Additionally, we assume access to a set of M models or “teachers” $\{h_i\}_{i=1}^M$ (e.g. publicly available pretrained models). We operate in the blind ensemble setting where we lack ground truth to evaluate teacher performance for model selection. To train f_θ , we propose to adaptively distill knowledge from the ensemble of teachers. Fig. 2 shows that each teacher has unique failure modes. To address this, we propose a monitored distillation framework for ensemble learning that employs positive congruent training: we only learn from a teacher if its predictions are compatible with the observed scene.

To this end, we leverage geometric constraints between I_t and $I_\tau \in I_T$ and validate the correctness of predictions $d_i := h_i(I_t, z_t)$ produced by each teacher through averaging their photometric reprojection residual from different views I_T . From the error, we derive a confidence map that determines the compatibility of each teacher to the observed image I_t . We then construct distilled depth $\bar{d} \in \mathbb{R}_+^{H \times W}$ via pixel-wise selection from the ensemble that yields the highest con-

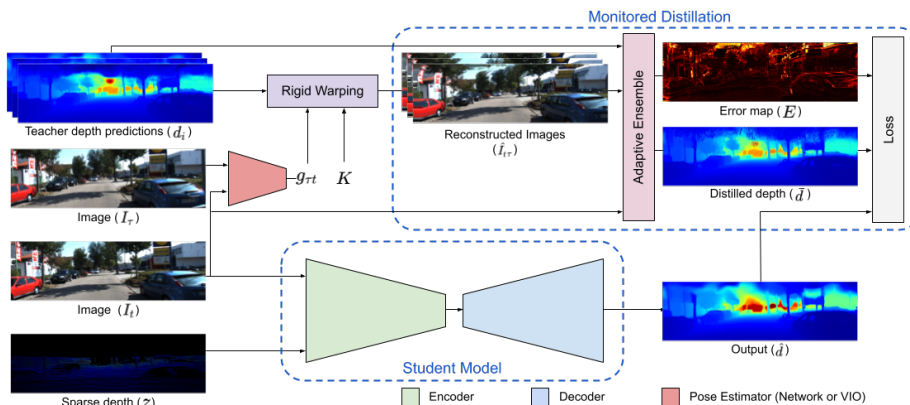


Fig. 1: **Monitored Distillation.** The student model (KBNet with depthwise separable convolutions) takes in the image I_t , the corresponding sparse depth map z , and camera intrinsics K to predict a dense depth map \hat{d} . Monitored distillation constructs the distilled depth \bar{d} via pixel-wise selection of the teacher’s predictions based on SSIM error. The combined error map E yields the monitor function Q for the loss which adaptively balances the monitored distillation loss from the ensemble and the unsupervised photometric and structural losses.

fidence. The resulting spatially varying confidence map acts as a “monitor” to balance the trade-off between “trusting” the ensemble and relying on photometric consistency as a supervisory signal (when all teachers yield high residuals).

3.1 Monitored Distillation

Given $M \in \mathbb{Z}^+$ teachers with respective output depth maps d_i , for $i \in \{1, \dots, M\}$, we aim to construct a distilled depth \bar{d} by adaptively selecting predictions from the teacher ensemble through comparing the structural similarity of an image I_t and its reprojection $\hat{I}_{t\tau}$ from an adjacent view $I_\tau, \tau \in T$ given by

$$\hat{I}_{t\tau}(x, d) = I_\tau(\pi g_{\tau t} K^{-1} \bar{x} d(x)), \quad (1)$$

where d denotes the depth values for $x \in \Omega$, $\bar{x} = [x^\top \ 1]^\top$ is the homogeneous coordinate of x , $g_{\tau t} \in SE(3)$ is the relative pose of the camera from view t to τ , K is the camera intrinsics, and π is the perspective projection. In practice, $g_{\tau t}$ can be derived from camera baseline if I_t and I_τ are stereo pairs, directly estimated by a visual inertial odometry (VIO) system, or learned from a pose network if the views are taken from a video.

For each teacher i , we measure the photometric reprojection error E_i via the mean SSIM [50] between I_t and each reconstruction $\hat{I}_{t\tau}(x, d_i), \tau \in T$:

$$E_i(x) = \frac{1}{|T|} \sum_{\tau \in T} (1 - \phi(\hat{I}_{t\tau}(x, d_i), I_t(x))) \quad (2)$$

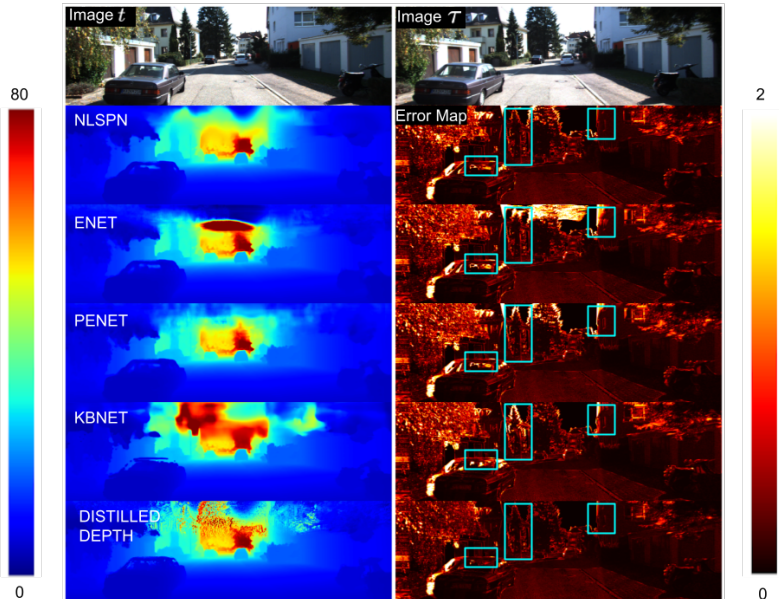


Fig. 2: **Error modes** for NLSPN, ENet, PENet, and KBNet on KITTI. The first row shows the input image I_t (left) and another view I_τ (right). Rows 2-5 are the respective teacher models’ dense depth maps (left) and reprojection error maps (right) that show different teacher models have different error modes. Row 6 shows **the distilled depth** which is adaptively constructed from depth outputs of teacher models. The error for each region in the distilled depth lower bounds the reprojection error of the individual teachers.

For ease of notation, we denote SSIM as $\phi(\cdot)$. To construct the distilled depth, we selectively choose the depth prediction for each pixel $x \in \Omega$ that minimizes the overall residual error across all teachers. Formally,

$$\bar{d}(x) = \sum_{i=1}^M \mathbb{1}_i(x) d_i(x), \quad (3)$$

where $\mathbb{1}_i$ is a binary weight map of the teacher i is given by

$$\mathbb{1}_i(x) = \begin{cases} 1 & E_i(x) < E_j(x) \forall j \neq i \\ 0 & \text{otherwise.} \end{cases} \quad (4)$$

In other words, $\mathbb{1}_i(x) = 1$ when $d_i(x)$ yields the lowest photometric residual. Fig. 3 shows the distribution of teachers chosen across difference depth ranges to construct the distilled depth. As observed, different teachers perform well in different regions. Our method selects points from each teacher with the lowest error (i.e. highest confidence) to yield an adaptive ensemble (see Fig. 2).

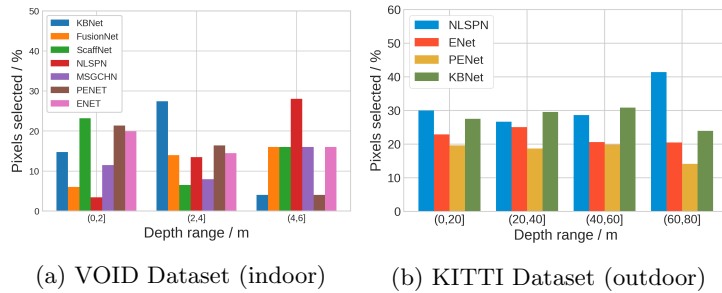


Fig. 3: Pixel Selection Distribution. The plot reflects the proportion of pixels from each teacher model selected for the ensemble for two different datasets. We observe that error modes of a teacher can vary across different depth ranges, demonstrated by the changing distribution of selected teachers.

Despite being trained on ground truth, each teacher can only *approximate* the true distribution of depths in the scene. While selectively ensembling based on the reprojection residual will address *some* error modes of the teachers, it is still possible for all teachers to yield high photometric residuals. Hence, we do not trust the ensemble fully, and instead further adaptively weight the ensemble supervision with a monitor Q based on the error of the distilled depth \bar{d} . As we have already constructed the error maps E_i for each teacher, we can similarly aggregate the error for each pixel $E(x) = \min_i E_i(x)$ for $x \in \Omega$. The monitor $Q \in [0, 1]^{H \times W}$ is a spatially adaptive per-pixel confidence map:

$$Q(x) = \exp(-\lambda E(x)), \quad (5)$$

where λ is the temperature parameter (see Sec. 4.1). Q naturally assigns higher confidence to points in the distilled depth that are compatible with the observed image I_t as measured by reprojection error, and is used to weight the supervision signal. Our monitored knowledge distillation objective reads:

$$\ell_{md} = \frac{1}{|\Omega|} \sum_{x \in \Omega} Q(x) \cdot |\hat{d}(x) - \bar{d}(x)|. \quad (6)$$

A student typically learns the error modes of its teacher. Thus by distilling from the adaptive ensemble of teachers that is positive congruent [57], our student model learns not to make the same mistake as any individual teacher. We refer to this process as Monitored Distillation, in which our monitor function Q gives higher weight to the teachers for regions lower reconstruction error. We default to unsupervised loss for regions where the ensemble yield high residuals to avoid learning the common error modes of the teachers.

3.2 Unsupervised objective

For regions with high reconstruction error, the monitoring function Q allows us to rely on standard unsupervised photometric reprojection error as our training

objective. Photometric reprojection loss comprises (1) ℓ_{co} , an L_1 penalty on color discrepancies between I_t and its reconstruction $I_{t\tau}$ and (2) structural loss ℓ_{st} :

$$\ell_{co} = \frac{1}{|T|} \frac{1}{|\Omega|} \sum_{x \in \Omega} \sum_{\tau \in T} (1 - Q(x)) (|\hat{I}_{t\tau}(x, \hat{d}) - I_t(x)|) \quad (7)$$

$$\ell_{st} = \frac{1}{|T|} \frac{1}{|\Omega|} \sum_{x \in \Omega} \sum_{\tau \in T} (1 - Q(x)) (1 - \phi(\hat{I}_{t\tau}(x, \hat{d}), I_t(x))) \quad (8)$$

We weight the relative contributions of these losses with the complement of our adaptive monitor function $(1 - Q)$. As a result, our framework naturally allows us to search for the correct correspondences (and in turn better depth estimation) in regions where the ensemble failed. In other words, regions which the monitor deems as high confidence are more heavily influenced by ℓ_{md} as supervision, while lower confidence regions will minimize unsupervised losses instead.

We note that the ensemble of teachers are typically regularized i.e. with local smoothness “baked in”. This presents an advantage: Since the ensemble is informed by large amounts of data, it learns the regularities in our physical world e.g. roads are flat and surfaces are locally smooth. Hence, the student model will naturally distill these priors (often too complex to be modeled by generic assumptions) from the ensemble. However, to account for cases where regularities provided are insufficient, such as when all teachers yields high reprojection errors on a given scene and hence defaults to unsupervised losses, we impose the default local smoothness regularizer as used in [35,44,51,53,54,58]:

$$\ell_{sm} = \frac{1}{|\Omega|} \sum_{x \in \Omega} \lambda_X(x) |\partial_X \hat{d}(x)| + \lambda_Y(x) |\partial_Y \hat{d}(x)| \quad (9)$$

where ∂_X, ∂_Y are gradients along the x and y directions, weighted by $\lambda_X := e^{-|\partial_X I_t(x)|}$ and $\lambda_Y := e^{-|\partial_Y I_t(x)|}$ respectively.

Thus, we have the following overall loss function

$$\mathcal{L} = w_{md} \ell_{md} + w_{ph} \ell_{ph} + w_{st} \ell_{st} + w_{sm} \ell_{sm} \quad (10)$$

where $w_{(\cdot)}$ denotes the respective weights for each loss term (see Sec. 4.1).

3.3 Student Model Architecture

Through monitored distillation from an ensemble of teachers, we note that a simpler student model can be trained on the output distribution of more complex teacher models to achieve comparable performance. Therefore, we condense KBNNet [54] by replacing the final two layers in the encoder with depth-wise separable convolutions [18] to yield a 23.2% reduction in number of model parameters. Compared to the best supervised teacher models that require 25.84M (NLSPN [37]), 131.7M (ENet [20]), 132M (PENet [20]), and the original KBNNet model with 6.9M parameters, our student model only requires 5.3M.

Table 1: **Blind ensemble distillation comparisons.** We compare Monitored Distillation to other naive ensembling methods. The supervised ensemble consists of NLSPN [37], MSG-CHN [30], ENet, and PENet [20]. The unsupervised ensemble consists of teachers trained on non-synthetic (FusionNet [51], KBNNet [54]), and synthetic (ScaffNet [51]) data. The heterogeneous ensemble consists of all seven methods. (*) refers to training without unsupervised losses. We include unsupervised losses in all other baselines and our approach. “Ours - Global” refers to selecting teachers based on global (as opposed to pixel-wise) residual

Ensemble Type	Method	MAE	RMSE	iMAE	iRMSE
None	KBNNet [54]	39.80	95.86	21.16	49.72
	Baseline Student	55.67	117.21	28.68	58.31
Supervised	Distill Mean (*)	34.27	91.72	17.63	41.39
	Distill Mean	34.04	89.19	17.30	40.43
	Distill Median	34.64	89.80	17.46	39.77
	Distill Random	35.18	92.30	18.41	42.95
	Ours	32.86	85.53	16.44	39.14
Unsupervised	Distill Mean (*)	44.73	96.56	24.08	49.55
	Distill Mean	41.96	94.47	23.80	50.37
	Distill Median	43.86	99.46	23.62	50.85
	Distill Random	39.38	92.14	20.62	46.04
	Ours (No synthetic)	40.10	92.03	22.16	46.86
	Ours	38.78	90.72	20.53	45.91
Heterogeneous	Distill Mean (*)	44.53	100.59	23.33	48.36
	Distill Mean	35.79	84.78	18.65	42.90
	Distill Median	33.89	85.25	17.31	40.40
	Distill Random	43.64	94.38	24.74	50.27
	Ours - Global	34.27	91.72	17.63	41.39
	Ours	32.09	80.20	16.15	38.86

4 Experiments

We evaluate our method on public benchmarks – VOID [53] for indoor and outdoor scenes and KITTI [46] for outdoor driving settings. We describe the error metrics used for evaluation in Supp. Mat. We assume the blind ensemble setting, in which we lack access to ground truth and hence are unable to evaluate the performance of individual teachers in the ensemble for model selection.

4.1 Implementation Details

We implement our approach in PyTorch. For both VOID and KITTI experiments, we set the temperature $\lambda = 0.1$ and the weights for the overall loss terms $w_{md} = 1.0, w_{ph} = 0.15, w_{st} = 0.85, w_{sm} = 0.1$. For the student baseline (without teachers), we emulate the training procedure of [54]. To obtain pose, we trained a pose network jointly with our depth model by minimizing Eqn. 10. For detailed training and augmentation schedules, please see Supp. Mat.

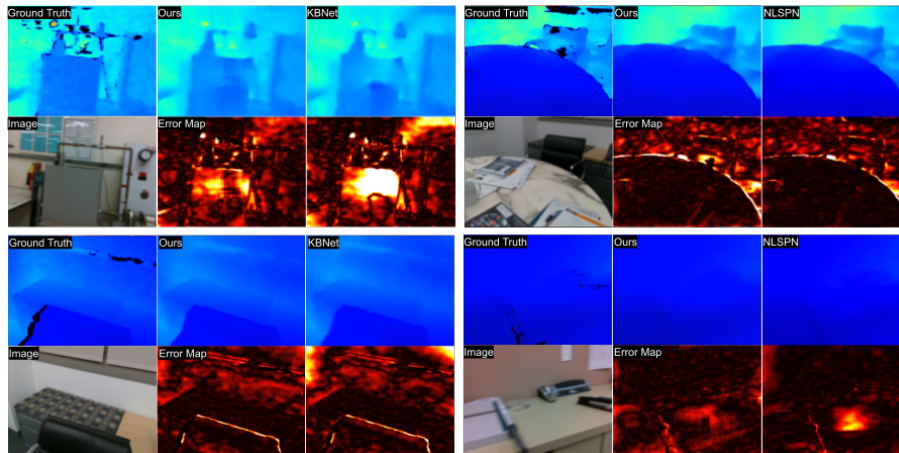


Fig. 4: **Monitored Distillation vs. unsupervised (left) and supervised (right) teachers.** While KBNet [54] is the best performer among unsupervised methods, by ensembling it with weaker methods, we addressed its error modes on lab equipment (top left). Similarly, we address the failure modes in the top supervised method NLSPN [37] by distilling from a heterogeneous ensemble.

4.2 Datasets

VOID [53] contains synchronized 640×480 RGB images and sparse depth maps of indoor (laboratories, classrooms, office spaces) and outdoor (gardens) scenes. The associated sparse depth maps contain ≈ 1500 sparse depth points with a density of $\approx 0.5\%$. They are obtained by a set of features tracked by XIVO [13], a VIO system. The dense ground-truth depth maps are acquired by active stereo. As opposed to static scenes in KITTI, the VOID dataset contains 56 sequences with challenging motion. Of the 56 sequences, 48 sequences ($\approx 45,000$ frames) are designated for training and 8 for testing (800 frames). We follow the evaluation protocol of [53] and cap the depths between 0.2 and 5.0 meters.

KITTI [46] depth completion benchmark contains $\approx 86,000$ raw 1242×375 image frames (43K stereo pairs) and synchronized sparse depth maps. The sparse depth is obtained using a Velodyne lidar sensor and, when projected, covers $\approx 5\%$ of the image space. The ground truth depths are semi-dense, which we use only for evaluation purposes. We use the designated 1,000 samples for validation and evaluate test-time accuracy on KITTI’s online testing server.

4.3 VOID Depth Completion Benchmark

We present qualitative and quantitative experiments on VOID against blind ensemble distillation baselines, and top supervised and unsupervised methods.

Distilling from Blind Ensemble. As we are the first to propose distillation for the blind ensemble setting, in Table 1, we compare our approach to

Table 2: **Comparison on VOID test set.** We compare against Unsupervised (U), Supervised (S), and Blind Ensemble (BE) methods. Our method outperforms all existing works except for [37] which has almost $5\times$ the number of parameters. Applying Monitored Distillation to the unsupervised ensemble also ranks first among unsupervised methods

Method	Type	# Param	Time	MAE	RMSE	iMAE	iRMSE
SS-S2D [35]	U	27.8M	59ms	178.85	243.84	80.12	107.69
DDP [58]	U	18.8M	54ms	151.86	222.36	74.59	112.36
VOICED [53]	U	9.7M	29ms	85.05	169.79	48.92	104.02
ScaffNet [51]	U	7.8M	25ms	59.53	119.14	35.72	68.36
ENet [20]	S	131.7M	75ms	46.90	94.35	26.78	52.58
MSG-CHN [30]	S	364K	36ms	43.57	109.94	23.44	52.09
KBNet [54]	U	6.9M	13ms	39.80	95.86	21.16	49.72
Ours (Unsupervised)	BE	5.3M	13ms	38.78	90.72	20.53	45.91
PENet [20]	S	132M	226ms	34.61	82.01	18.89	40.36
Ours (Supervised)	BE	5.3M	13ms	32.86	85.53	16.44	39.14
Ours (Heterogeneous)	BE	5.3M	13ms	32.09	80.20	16.15	38.86
<i>NLSPN [37]</i>	<i>S</i>	<i>25.8M</i>	<i>122ms</i>	<i>26.74</i>	<i>79.12</i>	<i>12.70</i>	<i>33.88</i>

baseline methods: (1) mean of teachers, (2) median of teachers, and (3) randomly selecting a teacher for each sample per iteration. We utilize ensembles comprising teachers trained with supervised and unsupervised methods (termed *supervised* and *unsupervised teachers* respectively), and teachers trained on synthetic data. Note that while we evaluate our method across different ensemble compositions, Monitored Distillation and baselines have no knowledge regarding any individual teacher in the ensemble and hence operate in the blind ensemble setting. For comparison purposes, scores for each teacher can be found in Table 2.

In the first section of Table 1, we show the baseline performance of the student network trained only on unsupervised losses. Rows 1-2 shows that shrinking KBNet [54] by 23.2% causes a sharp performance drop in the baseline student due to decrease in capacity. Next, we present results for distilling from an ensemble of supervised teachers: NLSPN [37], MSG-CHN [30], ENet, and PENet [20]. In this setting, our method outperforms naive ensemble distillation baselines by an average of 5.5%. We observe a similar performance gain when we distill from an ensemble of unsupervised (KBNet [54], FusionNet [51]) and synthetic (ScaffNet [51]) teachers. In this setting, our method outperforms naive ensemble baselines by an average of 6.8%. Notably, when we incorporate ScaffNet, which is “weaker”, or performs comparably worse than KBNet and FusionNet, we improve upon the ensemble without synthetic teachers by 3.5% on average.

When using Monitored Distillation to distill from a heterogeneous ensemble of teachers (containing the above 7 teachers), we observe this same trend where adding weaker teachers produces a stronger overall ensemble. Comparing super-

Table 3: **KITTI unsupervised depth completion benchmark.** Our method outperforms all unsupervised methods across all metrics on the KITTI leaderboard. * denotes methods that use additional synthetic data for training

Method	# Param	Time	MAE	RMSE	iMAE	iRMSE
SS-S2D [35]	27.8M	80ms	350.32	1299.85	1.57	4.07
IP-Basic [27]	0	11ms	302.60	1288.46	1.29	3.78
DFuseNet [44]	n/a	80ms	429.93	1206.66	1.79	3.62
DDP* [58]	18.8M	80ms	343.46	1263.19	1.32	3.58
VOICED [53]	9.7M	44ms	299.41	1169.97	1.20	3.56
AdaFrame [52]	6.4M	40ms	291.62	1125.67	1.16	3.32
SynthProj* [34]	2.6M	60ms	280.42	1095.26	1.19	3.53
ScaffNet* [51]	7.8M	32ms	280.76	1121.93	1.15	3.30
KBNet [54]	6.9M	16ms	256.76	1069.47	1.02	2.95
Ours	5.3M	16ms	218.60	785.06	0.92	2.11

vised vs. heterogeneous ensembles in naive distillation, adding weaker teachers results in a drop in performance as shown in Table 1. On the other hand, not only does Monitored Distillation discard the low-confidence predictions of weaker teachers, but it also leverages their strengths to correct certain error modes of the ensemble. Thus, even when the ensemble is “polluted” with weaker teachers, our robust method achieves strong performance across all metrics. On average, our method improves by 13.5% over baseline heterogeneous methods, and by 2.8% and 16.4% over Monitored Distillation using ensembles of only supervised and unsupervised teachers respectively. We further note that selecting a teacher based on the global reprojection error, labeled “Ours - Global” in Table 1, is less effective than constructing the distilled depth from the ensemble of teachers using a pixel-wise selection criterion.

Benchmark Comparisons. Table 2 shows comparisons against top supervised and unsupervised methods on VOID. In an indoor setting, point clouds are typically in orders of hundreds to several thousand points. As such, models become increasingly sensitive to the sparse depth map input, and in particular the distribution of sparse point within it. Additionally, indoor scene layouts are very complex, and there are many suitable dense representations that can complete a given point cloud. Hence, the accuracy of the model hinges on the regularization as most of the scene does not allow for establishing unique correspondences due to largely homogeneous regions, occlusions and the aperture problem.

Unlike generic regularizers such as piecewise-smoothness and local connectivity, our regularizer is informed by the statistics of many other scenes. Despite the unsupervised ensemble not containing methods that outperform the unsupervised state of the art [54], applying Monitored Distillation outperforms it by an average of 20.3% over all metrics while using a 23.2% smaller model. This shows that Monitored Distillation effectively leverages positive-congruency

Table 4: **KITTI supervised depth completion benchmark.** We compare against Distilled (D), Supervised (S), and Blind Ensemble (BE) methods. In this table, a method outranks another if it performs better on more than two metrics. Despite operating in the blind ensemble distillation regime, our method beats many supervised methods and our iMAE (0.92) and iRMSE (2.11) score are ranked 4th, and we are tied for 5th overall amongst supervised methods

Rank	Method	Type	MAE	RMSE	iMAE	iRMSE
15	ADNN [8]	S	439.48	1325.37	3.19	59.39
14	Morph-Net [10]	S	310.49	1045.45	1.57	3.84
13	CSPN [7]	S	279.46	1019.64	1.15	2.93
12	SS-S2D [35]	S	249.95	814.73	1.21	2.80
9	Self-Distill [22]	D	248.22	949.85	0.98	2.48
9	DeepLiDAR [40]	S	226.50	758.38	1.15	2.56
9	PwP [56]	S	235.73	785.57	1.07	2.52
8	UberATG-FuseNet [5]	S	221.19	752.88	1.14	2.34
5	Ours	BE	218.60	785.06	0.92	2.11
5	RGB_guide&certainty [47]	S	215.02	772.87	0.93	2.19
5	ENet [20]	S	216.26	741.30	0.95	2.14
4	PENet [20]	S	210.55	730.08	0.94	2.17
2	DDP [58]	S	203.96	832.94	0.85	2.10
2	CSPN++ [6]	S	209.28	743.69	0.90	2.07
1	NLSPN [37]	S	199.59	741.68	0.84	1.99

to produce a distillation objective that addresses the error modes of individual teachers. This is shown in Fig. 4 (top left), where we fixed the error modes in the lab equipment, and reduced errors in homogeneous regions.

Distilling from a heterogeneous ensemble yields a student that ranks 2nd on the benchmark, achieving comparable performance to the top method NLSPN [37] while using 79% less parameters. We show qualitatively in Fig. 4 that our model distills complex priors from the teacher ensemble regarding the topology of indoor surfaces, e.g. cabinets and tables are flat. On the bottom right of Fig. 4, we can even produce a more accurate depth estimate than NLSPN. These results show that Monitored Distillation is able to yield a positive congruent training by ensembling the strengths of individual teachers.

4.4 KITTI Depth Completion Benchmark

We run our method on the KITTI dataset using PENet, ENet[20], NLSPN[37], and KNet[54] as our heterogeneous ensemble. We compare our method against unsupervised and supervised depth completion methods quantitatively on the KITTI test set. We also provide qualitative comparisons in Supp. Mat.

Comparison with Unsupervised Methods. In Table 3, we demonstrate that despite having fewer parameters than most unsupervised models (e.g. 23.2% decrease compared to KNet[54], 73.0% decrease compared to DDP[58]), our method outperforms the state of the art [54] across all metrics by an average of 19.93%, where we improve by 14.86% in MAE, 26.59% in RMSE, 9.80% in iMAE, and 28.47% in iRMSE. Furthermore, our light-weight student model also boasts a 16ms inference time, which is comparable to [54]. Compared to methods that use synthetic ground truth to obtain a learned prior (marked with * in Table 3), our method leverages learned priors from pretrained models and improves over [34,51] by an average of 28.32% and 27.06%. We posit that this is largely due to the sim2real domain gap that [34,51,58] have to overcome i.e. covariate shift due to image translation error during training.

Comparison with Supervised Methods. We compare our method (having at best *indirect* access to ground truth) against supervised methods that have *direct* access to ground truth in training. Table 4 presents quantitative comparisons against supervised methods. We rank 4th in iMAE and iRMSE, and tie for 5th overall. Compared to knowledge distillation method [22], we beat them by 12.6% despite (1) them using ground truth and (2) applying our method in the blind ensemble setting. We achieve comparable performance to the teacher models ENet [20] (131.7M params), PENet [20] (132M params), and NLSPN [37] (25.8M params) across all metrics despite only requiring 5.3M parameters.

5 Discussion

We propose a method for blind ensemble learning and knowledge distillation on depth completion tasks. Our method is capable of shrinking model size by 79% compared to the best teacher model, while still attaining comparable performance, enabling lightweight and deployable models. The ensemble is curated by Monitored Distillation: a pixel-wise selection from the predictions of multiple teachers using reprojection error as a criteria. Because each teacher model has distinct failure modes, our ensemble alleviates the error inherited by the student model, improving performance compared to utilizing a single teacher or a naive mean ensemble. Still, there exist areas where all teachers have high uncertainty (e.g. further regions or areas of occlusion). In these cases, we cannot trust any teacher’s prediction. Instead, we employ a monitoring function to adaptively weight the distilled depth to increase the contribution of unsupervised losses.

However, we note that learning distilled regularities from teachers imposes several risks and limitations. First, the ability of our method to outperform unsupervised training methods relies on the composition of teachers and their error modes. If all teachers perform poorly on certain regions, our performance in these regions will not improve beyond training with unsupervised losses. Second, the method relies on unsupervised photometric and structural losses. If there is not enough parallax between the stereo images or movement between the image frames in the monocular setting, the photometric reprojection is uninformative regarding the depth of the scene. Third, reprojection error is limited when Lam-

bertian assumptions are violated. However, we know from [24] that the domain coverage of specularities and translucency is sparse due to the sparsity of primary illuminants (rank of the reflectance tensor is deficient and typically small). So, explicitly modeling deviations from diffuse Lambertian reflection is likely to yield modest returns.

We foresee this method being applied to many geometric problems (e.g. optical flow, stereo, and multiview geometry). Our method is the first attempt in blind ensemble distillation to produce positive congruent students, and we hope it lays the groundwork for monitored approaches leveraging the abundance of existing pretrained models.

References

1. Chao, C.H., Cheng, B.W., Lee, C.Y.: Rethinking ensemble-distillation for semantic segmentation based unsupervised domain adaption. In: Proceedings of the IEEE/CVF Conference on Computer Vision and Pattern Recognition. pp. 2610–2620 (2021)
2. Chawla, A., Yin, H., Molchanov, P., Alvarez, J.: Data-free knowledge distillation for object detection. In: Proceedings of the IEEE/CVF Winter Conference on Applications of Computer Vision. pp. 3289–3298 (2021)
3. Chen, G., Choi, W., Yu, X., Han, T., Chandraker, M.: Learning efficient object detection models with knowledge distillation. *Advances in neural information processing systems* **30** (2017)
4. Chen, L., Yu, C., Chen, L.: A new knowledge distillation for incremental object detection. In: 2019 International Joint Conference on Neural Networks (IJCNN). pp. 1–7. IEEE (2019)
5. Chen, Y., Yang, B., Liang, M., Urtasun, R.: Learning joint 2d-3d representations for depth completion. In: Proceedings of the IEEE International Conference on Computer Vision. pp. 10023–10032 (2019)
6. Cheng, X., Wang, P., Guan, C., Yang, R.: Cspn++: Learning context and resource aware convolutional spatial propagation networks for depth completion. In: Proceedings of the AAAI Conference on Artificial Intelligence. vol. 34, pp. 10615–10622 (2020)
7. Cheng, X., Wang, P., Yang, R.: Depth estimation via affinity learned with convolutional spatial propagation network. In: Proceedings of the European Conference on Computer Vision (ECCV). pp. 103–119 (2018)
8. Chodosh, N., Wang, C., Lucey, S.: Deep convolutional compressed sensing for lidar depth completion. In: Asian Conference on Computer Vision. pp. 499–513. Springer (2018)
9. Choi, K., Jeong, S., Kim, Y., Sohn, K.: Stereo-augmented depth completion from a single rgb-lidar image. In: 2021 IEEE International Conference on Robotics and Automation (ICRA). pp. 13641–13647. IEEE (2021)
10. Dimitrievski, M., Veelaert, P., Philips, W.: Learning morphological operators for depth completion. In: International Conference on Advanced Concepts for Intelligent Vision Systems. Springer (2018)
11. Eldesokey, A., Felsberg, M., Holmquist, K., Persson, M.: Uncertainty-aware cnns for depth completion: Uncertainty from beginning to end. In: Proceedings of the IEEE/CVF Conference on Computer Vision and Pattern Recognition. pp. 12014–12023 (2020)

12. Eldesokey, A., Felsberg, M., Khan, F.S.: Propagating confidences through cnns for sparse data regression. In: Proceedings of British Machine Vision Conference (BMVC) (2018)
13. Fei, X., Wong, A., Soatto, S.: Geo-supervised visual depth prediction. IEEE Robotics and Automation Letters **4**(2), 1661–1668 (2019)
14. Fischler, M.A., Bolles, R.C.: Random sample consensus: a paradigm for model fitting with applications to image analysis and automated cartography. Communications of the ACM **24**(6), 381–395 (1981)
15. Fukuda, T., Suzuki, M., Kurata, G., Thomas, S., Cui, J., Ramabhadran, B.: Efficient knowledge distillation from an ensemble of teachers. In: Interspeech. pp. 3697–3701 (2017)
16. Gofer, E., Praisler, S., Gilboa, G.: Adaptive lidar sampling and depth completion using ensemble variance. IEEE Transactions on Image Processing (2021)
17. Hinton, G., Vinyals, O., Dean, J.: Distilling the knowledge in a neural network. arXiv preprint arXiv:1503.02531 (2015)
18. Howard, A.G., Zhu, M., Chen, B., Kalenichenko, D., Wang, W., Weyand, T., Andreetto, M., Adam, H.: Mobilenets: Efficient convolutional neural networks for mobile vision applications. arXiv preprint arXiv:1704.04861 (2017)
19. Hu, J., Fan, C., Jiang, H., Guo, X., Gao, Y., Lu, X., Lam, T.L.: Boosting light-weight depth estimation via knowledge distillation. arXiv preprint arXiv:2105.06143 (2021)
20. Hu, M., Wang, S., Li, B., Ning, S., Fan, L., Gong, X.: Penet: Towards precise and efficient image guided depth completion. arXiv preprint arXiv:2103.00783 (2021)
21. Huang, Z., Fan, J., Cheng, S., Yi, S., Wang, X., Li, H.: Hms-net: Hierarchical multi-scale sparsity-invariant network for sparse depth completion. IEEE Transactions on Image Processing **29**, 3429–3441 (2019)
22. Hwang, S., Lee, J., Kim, W.J., Woo, S., Lee, K., Lee, S.: Lidar depth completion using color-embedded information via knowledge distillation. IEEE Transactions on Intelligent Transportation Systems (2021)
23. Jaritz, M., De Charette, R., Wirbel, E., Perrotton, X., Nashashibi, F.: Sparse and dense data with cnns: Depth completion and semantic segmentation. In: 2018 International Conference on 3D Vision (3DV). pp. 52–60. IEEE (2018)
24. Jin, H., Soatto, S., Yezzi, A.J.: Multi-view stereo beyond lambert. In: 2003 IEEE Computer Society Conference on Computer Vision and Pattern Recognition, 2003. Proceedings. vol. 1, pp. I–I. IEEE (2003)
25. Kang, J., Gwak, J.: Ensemble learning of lightweight deep learning models using knowledge distillation for image classification. Mathematics **8**(10), 1652 (2020)
26. Kingma, D.P., Ba, J.L.: Adam: A method for stochastic gradient descent. In: ICLR: International Conference on Learning Representations (2015)
27. Ku, J., Harakeh, A., Waslander, S.L.: In defense of classical image processing: Fast depth completion on the cpu. In: 2018 15th Conference on Computer and Robot Vision (CRV). pp. 16–22. IEEE (2018)
28. Lan, X., Zhu, X., Gong, S.: Knowledge distillation by on-the-fly native ensemble. arXiv preprint arXiv:1806.04606 (2018)
29. Lepetit, V., Moreno-Noguer, F., Fua, P.: Epnnp: An accurate o (n) solution to the pnp problem. International journal of computer vision **81**(2), 155 (2009)
30. Li, A., Yuan, Z., Ling, Y., Chi, W., Zhang, C., et al.: A multi-scale guided cascade hourglass network for depth completion. In: Proceedings of the IEEE/CVF Winter Conference on Applications of Computer Vision. pp. 32–40 (2020)

31. Liu, Y., Chen, K., Liu, C., Qin, Z., Luo, Z., Wang, J.: Structured knowledge distillation for semantic segmentation. In: Proceedings of the IEEE/CVF Conference on Computer Vision and Pattern Recognition. pp. 2604–2613 (2019)
32. Liu, Y., Shu, C., Wang, J., Shen, C.: Structured knowledge distillation for dense prediction. *IEEE transactions on pattern analysis and machine intelligence* (2020)
33. Liu, Y., Sheng, L., Shao, J., Yan, J., Xiang, S., Pan, C.: Multi-label image classification via knowledge distillation from weakly-supervised detection. In: Proceedings of the 26th ACM international conference on Multimedia. pp. 700–708 (2018)
34. Lopez-Rodriguez, A., Busam, B., Mikolajczyk, K.: Project to adapt: Domain adaptation for depth completion from noisy and sparse sensor data. In: Proceedings of the Asian Conference on Computer Vision (2020)
35. Ma, F., Cavalheiro, G.V., Karaman, S.: Self-supervised sparse-to-dense: Self-supervised depth completion from lidar and monocular camera. In: International Conference on Robotics and Automation (ICRA). pp. 3288–3295. IEEE (2019)
36. Michieli, U., Zanuttigh, P.: Knowledge distillation for incremental learning in semantic segmentation. *Computer Vision and Image Understanding* **205**, 103167 (2021)
37. Park, J., Joo, K., Hu, Z., Liu, C.K., Kweon, I.S.: Non-local spatial propagation network for depth completion. In: European Conference on Computer Vision, ECCV 2020. European Conference on Computer Vision (2020)
38. Park, S., Heo, Y.S.: Knowledge distillation for semantic segmentation using channel and spatial correlations and adaptive cross entropy. *Sensors* **20**(16), 4616 (2020)
39. Pilzer, A., Lathuiliere, S., Sebe, N., Ricci, E.: Refine and distill: Exploiting cycle-inconsistency and knowledge distillation for unsupervised monocular depth estimation. In: Proceedings of the IEEE/CVF Conference on Computer Vision and Pattern Recognition. pp. 9768–9777 (2019)
40. Qiu, J., Cui, Z., Zhang, Y., Zhang, X., Liu, S., Zeng, B., Pollefeys, M.: Deeplidar: Deep surface normal guided depth prediction for outdoor scene from sparse lidar data and single color image. In: Proceedings of the IEEE Conference on Computer Vision and Pattern Recognition. pp. 3313–3322 (2019)
41. Qu, C., Liu, W., Taylor, C.J.: Bayesian deep basis fitting for depth completion with uncertainty. *arXiv preprint arXiv:2103.15254* (2021)
42. Qu, C., Nguyen, T., Taylor, C.: Depth completion via deep basis fitting. In: Proceedings of the IEEE/CVF Winter Conference on Applications of Computer Vision. pp. 71–80 (2020)
43. Romero, A., Ballas, N., Kahou, S.E., Chassang, A., Gatta, C., Bengio, Y.: Fitnets: Hints for thin deep nets. *arXiv preprint arXiv:1412.6550* (2014)
44. Shivakumar, S.S., Nguyen, T., Miller, I.D., Chen, S.W., Kumar, V., Taylor, C.J.: Dfusenet: Deep fusion of rgb and sparse depth information for image guided dense depth completion. In: 2019 IEEE Intelligent Transportation Systems Conference (ITSC). pp. 13–20. IEEE (2019)
45. Traganitis, P.A., Giannakis, G.B.: Blind multi-class ensemble learning with dependent classifiers. In: 2018 26th European Signal Processing Conference (EUSIPCO). pp. 2025–2029. IEEE (2018)
46. Uhrig, J., Schneider, N., Schneider, L., Franke, U., Brox, T., Geiger, A.: Sparsity invariant cnns. In: 2017 International Conference on 3D Vision (3DV). pp. 11–20. IEEE (2017)
47. Van Gansbeke, W., Neven, D., De Brabandere, B., Van Gool, L.: Sparse and noisy lidar completion with rgb guidance and uncertainty. In: 2019 16th International Conference on Machine Vision Applications (MVA). pp. 1–6. IEEE (2019)

48. Walawalkar, D., Shen, Z., Savvides, M.: Online ensemble model compression using knowledge distillation. In: European Conference on Computer Vision. pp. 18–35. Springer (2020)
49. Wang, Y., Li, X., Shi, M., Xian, K., Cao, Z.: Knowledge distillation for fast and accurate monocular depth estimation on mobile devices. In: Proceedings of the IEEE/CVF Conference on Computer Vision and Pattern Recognition. pp. 2457–2465 (2021)
50. Wang, Z., Bovik, A.C., Sheikh, H.R., Simoncelli, E.P.: Image quality assessment: from error visibility to structural similarity. *IEEE transactions on image processing* **13**(4), 600–612 (2004)
51. Wong, A., Cicek, S., Soatto, S.: Learning topology from synthetic data for unsupervised depth completion. *IEEE Robotics and Automation Letters* **6**(2), 1495–1502 (2021)
52. Wong, A., Fei, X., Hong, B.W., Soatto, S.: An adaptive framework for learning unsupervised depth completion. *IEEE Robotics and Automation Letters* **6**(2), 3120–3127 (2021)
53. Wong, A., Fei, X., Tsuei, S., Soatto, S.: Unsupervised depth completion from visual inertial odometry. *IEEE Robotics and Automation Letters* (2020)
54. Wong, A., Soatto, S.: Unsupervised depth completion with calibrated backprojection layers. In: Proceedings of the IEEE/CVF International Conference on Computer Vision. pp. 12747–12756 (2021)
55. Xiang, L., Ding, G., Han, J.: Learning from multiple experts: Self-paced knowledge distillation for long-tailed classification. In: European Conference on Computer Vision. pp. 247–263. Springer (2020)
56. Xu, Y., Zhu, X., Shi, J., Zhang, G., Bao, H., Li, H.: Depth completion from sparse lidar data with depth-normal constraints. In: Proceedings of the IEEE International Conference on Computer Vision. pp. 2811–2820 (2019)
57. Yan, S., Xiong, Y., Kundu, K., Yang, S., Deng, S., Wang, M., Xia, W., Soatto, S.: Positive-congruent training: Towards regression-free model updates. In: Proceedings of the IEEE/CVF Conference on Computer Vision and Pattern Recognition. pp. 14299–14308 (2021)
58. Yang, Y., Wong, A., Soatto, S.: Dense depth posterior (ddp) from single image and sparse range. In: Proceedings of the IEEE/CVF Conference on Computer Vision and Pattern Recognition. pp. 3353–3362 (2019)
59. Zhang, Y., Funkhouser, T.: Deep depth completion of a single rgb-d image. In: Proceedings of the IEEE Conference on Computer Vision and Pattern Recognition. pp. 175–185 (2018)

Monitored Distillation for Positive Congruent Depth Completion

SUPPLEMENTARY MATERIALS

6 Summary of Contents

In Sec. 7 we provide our hyperparameters and augmentations used during training. In Sec. 8, we provide a sensitivity study on the effect of sparsity in the input. In Sec. 9, we compare Monitored Distillation to methods operating under the non-blind ensemble setting and show that distilling from a blind ensemble using our method improves over directly distilling from any single teacher – even the best teacher. In Sec. 10 we make qualitative comparisons against the state-of-the-art unsupervised (Fig. 6, 7) and supervised methods (Fig. 8, 9) and show that our method achieves comparable performance to the top supervised methods while using significantly fewer parameters. We further include a discussion regarding the error modes of teacher models and show that Monitored Distillation is able to avoid distilling the error modes of individual teachers. Lastly, we conclude with a discussion on the limitations of our method in Sec. 11.

Table 5: **Learning rate schedule for KITTI (outdoors) and VOID (indoors) depth completion benchmark datasets.**

Epochs	Learning Rate
KITTI [46]	
0 to 30	5×10^{-4}
30 to 50	2×10^{-4}
50 to 90	5×10^{-5}
90 to 100	2×10^{-5}
VOID [53]	
0 to 15	5×10^{-4}
15 to 20	2×10^{-4}
20 to 50	5×10^{-5}

Table 6: **Min pool and max pool kernel sizes for our sparse-to-dense module.** Kernel sizes for VOID [53] are larger because the point cloud generated from VIO [13] is much sparser than that of the LIDAR used in KITTI [46]

Dataset	Min Pool	Max Pool
KITTI [46]	5, 7, 9, 11, 13	15, 17
VOID [53]	15, 17, 19, 21, 23	27, 29

Table 7: **Error metrics.** d_{gt} denotes ground truth depth.

Metric	Definition
MAE	$\frac{1}{ \Omega } \sum_{x \in \Omega} \hat{d}(x) - d_{gt}(x) $
RMSE	$(\frac{1}{ \Omega } \sum_{x \in \Omega} \hat{d}(x) - d_{gt}(x) ^2)^{1/2}$
iMAE	$\frac{1}{ \Omega } \sum_{x \in \Omega} 1/\hat{d}(x) - 1/d_{gt}(x) $
iRMSE	$(\frac{1}{ \Omega } \sum_{x \in \Omega} 1/\hat{d}(x) - 1/d_{gt}(x) ^2)^{1/2}$

7 Implementation Details

We optimized our networks using Adam [26] with $\beta_1 = 0.9$ and $\beta_2 = 0.999$. We trained for a total of 100 epochs on KITTI [46], and 50 epochs on VOID [53]. We use a batch size of 8 and choose $w_{md} = 1.0$, $w_{ph} = 0.15$, $w_{st} = 0.85$, $w_{sm} = 0.1$ and temperature parameter $\lambda = 0.10$ for both KITTI and VOID. We detail our learning rate schedule for each dataset in Table 5. We employ a sparse-to-dense module from [54], and the min and max pool kernel sizes are detailed in Table 6.

For data augmentations, we performed random horizontal and vertical crops to the image and depth map of size 768×320 for KITTI and 576×448 for VOID. We randomly removed between 60% to 70% of the sparse points for KITTI and 60% to 95% of the sparse points for VOID. For both KITTI and VOID, we performed random color shifts, saturation and contrast adjustments between 0.80 and 1.20 in the input. Augmentations are enabled 100% of the time for both KITTI and VOID. Each augmentation has a 50% chance of being applied.

For the ease of training, we preprocess both datasets by running inference on the training sets using each teacher model (except for sparse depth maps, which are given) and load them during training. We run heterogeneous experiments under two settings - taking one teacher from each (supervised, unsupervised, synthetic) category and using all 7 teachers - and report the best obtained result.

In Table 7 we present four metrics that we use to evaluate our models. These are the metrics reported on the KITTI and VOID benchmark datasets.

8 Sensitivity to Various Input Densities

To demonstrate robustness against varying levels of sparsity in the input, we evaluate our method on VOID using input sparse point clouds of varying densi-

Table 8: **Sensitivity study on various sparse depth density levels on VOID.** We train a single model on VOID using sparse depth maps of 0.50% density and evaluate it on 0.50%, 0.15%, 0.05% density test sets. On average, we outperform naive ensembling by 13.26% at 0.50% density, 19.60% at 0.15% density, and 26.52% at 0.05% density. Across all densities, we outperform naive ensembling on average by 19.79%.

Method	MAE	RMSE	iMAE	iRMSE
0.50% Density				
Distill Mean	35.791	84.780	18.651	42.899
Distill Median	33.889	85.245	17.296	40.401
Distill Random	43.638	94.384	24.741	50.265
Ours	32.094	80.196	16.154	38.856
0.15% Density				
Distill Mean	75.969	169.259	35.502	76.108
Distill Median	74.192	177.365	33.046	71.460
Distill Random	78.819	166.750	39.183	77.690
Ours	60.132	132.208	28.736	63.762
0.05% Density				
Distill Mean	139.676	281.677	64.233	119.177
Distill Median	139.276	306.621	57.785	109.511
Distill Random	129.900	259.239	62.354	111.820
Ours	93.814	186.970	46.990	92.830

ties: 150, 500, and 1500 points which correspond to densities of approximately 0.05%, 0.15%, and 0.5% respectively over the image space. Compared to datasets such as KITTI, sparse point clouds on VOID can be 100× more sparse, making sparse to dense depth completion even more challenging.

As expected, qualitative results shown in Fig. 5 demonstrate that our performance improves as density increases. We note that as the density of the point cloud decreases, more errors occur in far, homogeneous regions that tend to lack sparse points. In which case, we observe that our model is biased towards outputting farther depths. Quantitative results against naive blind ensembling baselines are provided in Table 8, where we restored the best checkpoint trained on 0.5% density for each model and evaluated on the VOID test set of 0.05%, 0.15% 0.5%. Our method consistently outperforms ensembling baselines on an average of 19.79% across all metrics, demonstrating greater improvement for lower densities. This suggests our method is robust to sparseness and less reliant

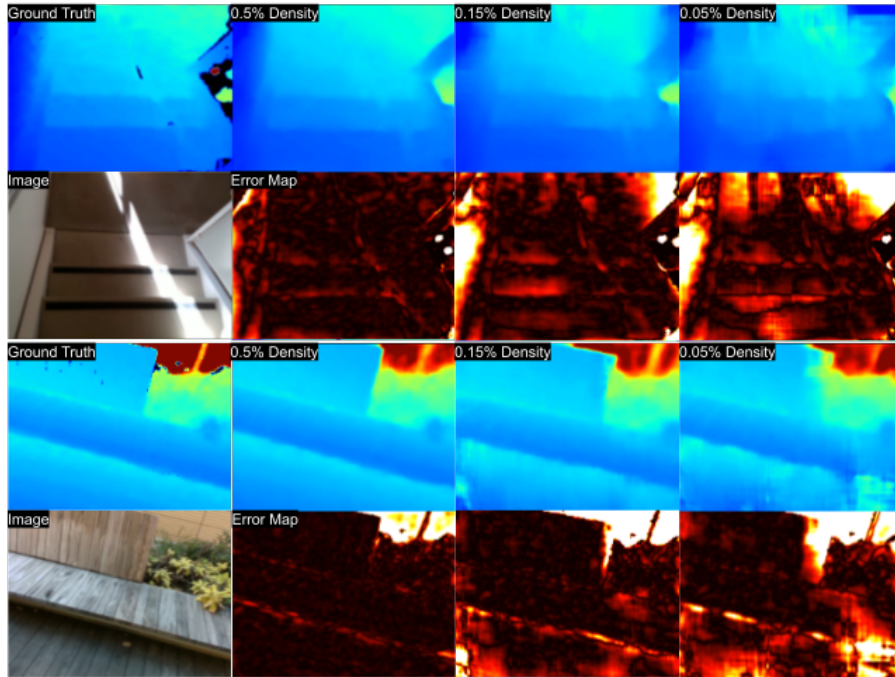


Fig. 5: **Qualitative results for density sensitivity study.** For two different samples (top half and bottom half), the left column shows the ground truth depth prediction and original image. The right three columns represent our method’s output predictions given sparse depth maps at 0.5%, 0.15% and 0.05% density. As observed, error increases with decreasing densities.

on sparse depth assistance. The use case is for densifying point clouds produced by VIO systems, where locally there are few or no points. Thus, learning a prior on the shapes of objects populating the scene becomes critical as the model must depend more on the information from the image.

However, we must note that, while our method beats others for each tested density levels, our model is also sensitive to the input density. Specifically, our mean error almost doubles ($\times 1.74$) when density decreases to 0.15% and almost triples ($\times 2.64$) when density decreases to 0.05% (i.e. decreases by 10x). This is shown quantitatively in Table 8 and qualitatively in Fig. 5 where far regions that are largely homogeneous become increasingly corrupted. This is because there are usually fewer or no points tracked by the VIO system in those areas.

9 Comparison to Non-blind Ensemble Baselines

We compare our results to naive methods run without the blind-ensemble assumption (i.e. the best performing model is known). We compare against the

Table 9: **Knowledge distillation benchmarks on KITTI validation set.** Unsupervised baseline (row 1) is trained on standard photometric reprojection loss. Distilling from the mean of the ensemble (row 2) yields union of the error modes. Single teacher distillation baselines (rows 3-5) improves upon the mean ensemble. The best performing method is our full model (row 6), where our monitored distillation boosts performance of the best model (NLSPN) even though we operate in the blind ensemble setting.

Method	MAE	RMSE	iMAE	iRMSE
Student Baseline	333.865	1374.013	1.315	4.260
Distill Mean	232.481	851.285	0.963	2.405
Distill E-Net [20]	228.356	831.737	0.952	2.278
Distill PE-Net [20]	226.058	819.46	0.964	2.316
Distill NLSPN [37]	221.077	841.952	0.921	2.234
Ours	218.222	815.157	0.910	2.184

baseline approach of simply training using the best performing teacher, and show that we perform better despite operating under the blind ensemble setting. We note that while many methods have proposed distilling from a single teacher, in many cases this is not practical. To determine which teacher to distill from, one must have a measure error; existing methods relied on ground truth to select the teacher model. Yet, in reality, ground truth is often not available and when available it is expensive to obtain. So without ground truth i.e. the blind ensemble setting, it becomes non-trivial to “find” the best teacher. For this particular scenario in Table 9, we assume competing methods are able to choose the best teacher and distill from them. This also serves as baseline for how well a student model distilling from any particular top method will perform.

In Table 9, we compare against using only unsupervised losses (baseline, row 1), the naive mean blind ensembling method with unsupervised loss (row 2), distilling from a single teacher (rows 3-5), and Monitored Distillation (last row). We observe that learning from an ensemble of teachers using the mean prediction (row 2) with unsupervised losses yield the union of error modes. In fact, distilling from the mean of the ensemble performs *worse* than distilling from any single teachers across all metrics. Furthermore, while knowledge distillation with a single teacher (rows 3-5) improves the baseline and also distilling from the mean of the ensemble, none of them produces the results that outperforms our method that distills from a blind ensemble since the student model may still propagate the teacher’s error modes.

We demonstrate the effectiveness of Monitored Distillation in row 6 of Table 9, where our model performs significantly better than the distilling from any of the individual teachers – even the best one, NLSPN [37]. Specifically, our monitor allows the model to adaptively choose the teachers that best minimize

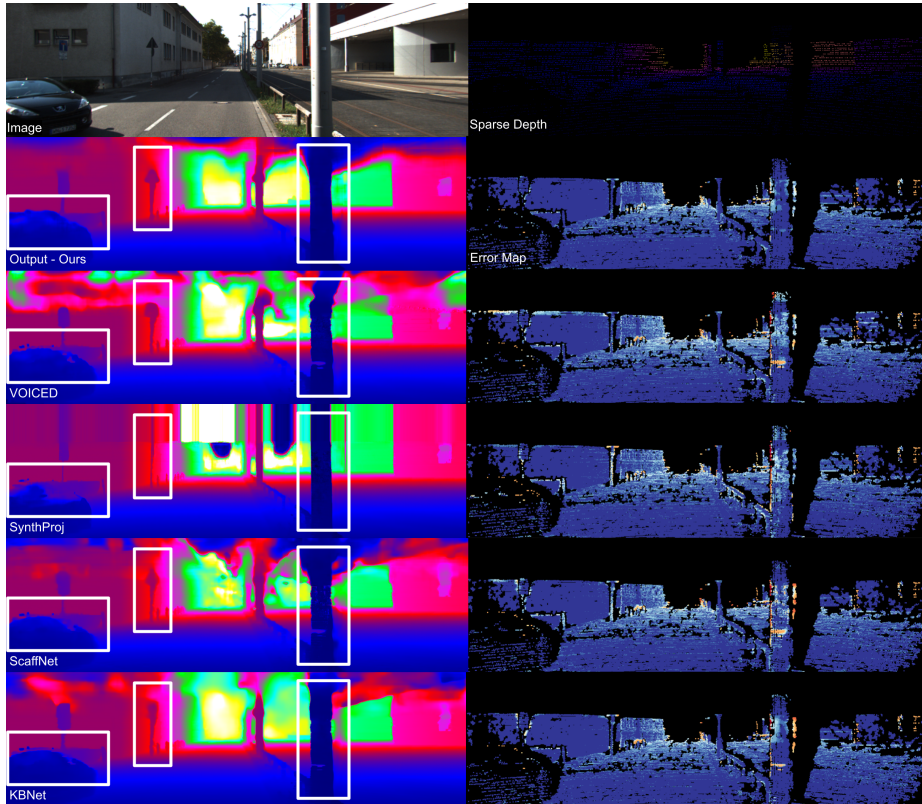


Fig. 6: **KITTI - Comparison to Unsupervised Methods #1** Monitored Distillation, VOICED [53], ScaffNet [51], SynthProj [34], KBNet [54]. The first row shows the input image I_t (left) and sparse depth z (right). Rows 2-5 are the respective models’ dense depth maps (left) and error maps w.r.t ground truth (right). The distilled regularization learnt by our approach improves accuracy for transparent/translucent regions like car windows, and structures such as poles. This is a known error mode of unsupervised methods due to the ambiguity of homogeneous surfaces.

reprojection residual (for calibrated images, the photometric reprojection error is a well-supported measure of reconstruction quality) and to fall back on unsupervised losses to learn the correct correspondences when the teachers fail to yield low reprojection residuals.

10 Qualitative Comparisons on KITTI

Here, we provide qualitative comparisons across the spectrum of supervision. First, we compare against top unsupervised methods on the KITTI benchmark,

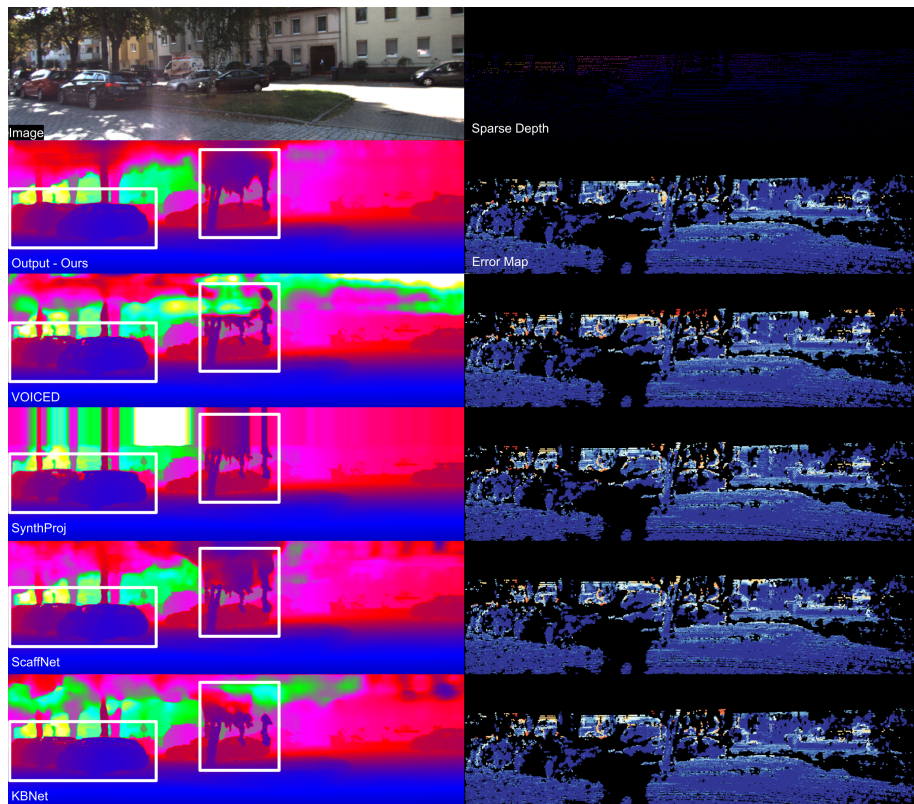


Fig. 7: **KITTI - Comparison to Unsupervised Methods #2** Monitored Distillation, VOICED [53], ScaffNet [51], SynthProj [34], KBNet [54]. The first row shows the input image I_t (left) and sparse depth z (right). Rows 2-5 are the respective models’ dense depth maps (left) and error maps w.r.t ground truth (right). The distilled regularization learnt by our approach improves accuracy for transparent/translucent regions like car windows, and complex structures like trees. This is a known error mode of unsupervised methods due to the ambiguity of homogeneous surfaces.

where we show that our method is able to better recover the complex and homogeneous structures. After that, we show head-to-head comparisons against the top supervised and unsupervised methods that we distill from and demonstrate that we yield positive congruent training as we avoid distilling from the error modes of individual teachers.

10.1 Against Unsupervised Methods

We qualitatively compare our results against top unsupervised methods in Fig. 6 and Fig. 7. We provide head-to-head comparisons against VOICED [53], ScaffNet

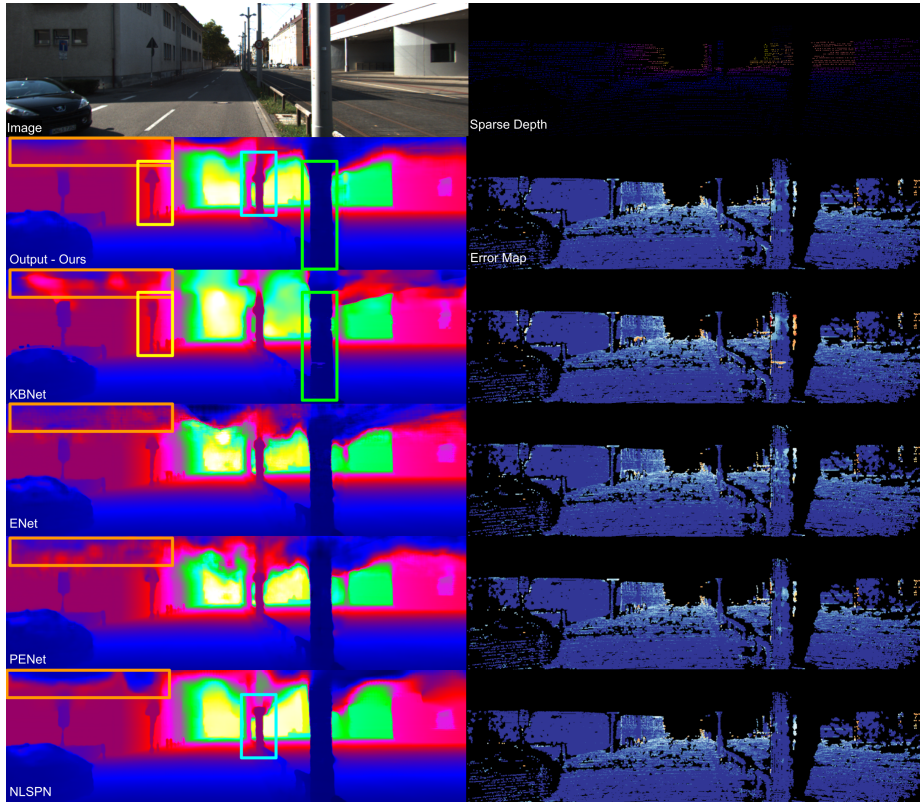


Fig. 8: **KITTI - Comparison to Teacher Methods #1** Monitored Distillation, KBNNet [54], PENet [20], ENet [20], and NLSPN [37]. The first row shows the input image I_t (left) and sparse depth z (right). Rows 2-5 are the respective models’ dense depth maps (left) and error maps w.r.t ground truth (right). We show that our method fixes (highlighted) error modes present in the teachers.

[51], SynthProj [34], KBNNet [54]. As demonstrated in our figures, the distilled regularization learned by our approach yields higher model accuracy overall, especially in transparent or translucent regions such as car windows, and largely homogeneous and thin structures like poles and trees. This shows that our Monitored Distillation approach can effectively distill priors learnt by the complex teacher networks to our lightweight student model. Compared against the state of the art [54], our method consistently yields lower error in vehicles, highlighted in white, where we do not suffer from the lidar artifacts leaving “holes” in the cars. In general, our method learns to produce consistent depths within an object for instance the pole and wall in the left image of Fig. 6 – [54] predicted a break in the pole whereas our method produces a continuous surface.

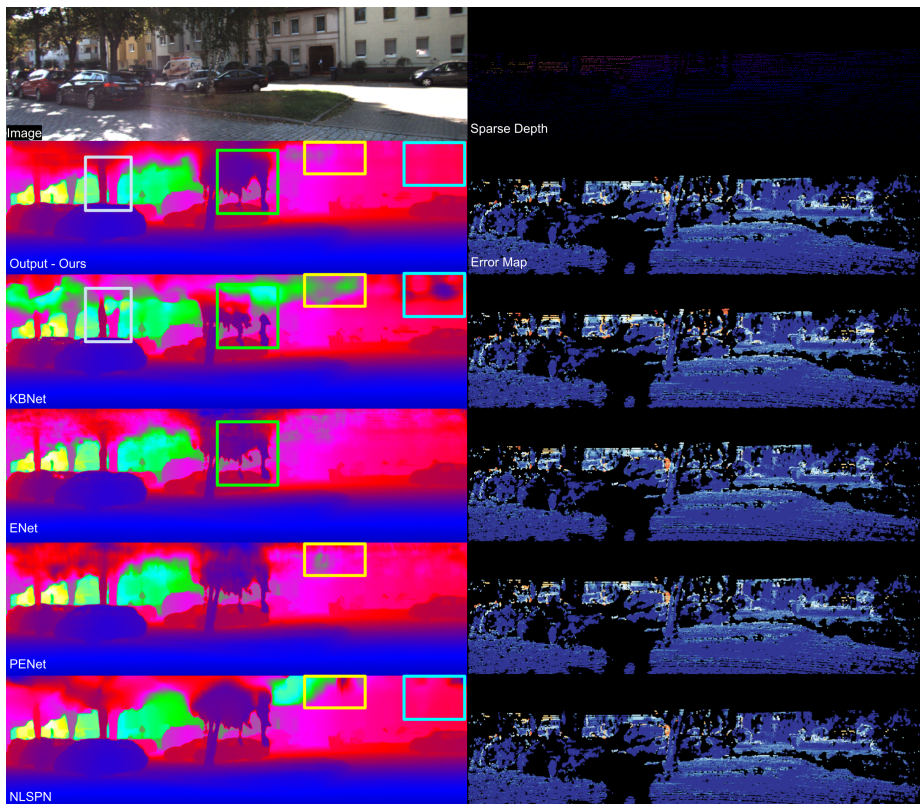


Fig. 9: **KITTI - Comparison to Teacher Methods #2** Monitored Distillation, KBNet [54], PENet [20], ENet [20], and NLSPN [37]. The first row shows the input image I_t (left) and sparse depth z (right). Rows 2-5 are the respective models’ dense depth maps (left) and error maps w.r.t ground truth (right). We show that our method fixes (highlighted) error modes present in the teachers.

10.2 Positive Congruent Training

In Fig. 8 and Fig. 9, we further compare the output of our method against the top supervised and unsupervised methods from which we distill our regularities: KBNet [54], PENet [20], ENet [20], and NLSPN [37]. Each teacher has some error modes. For instance, as highlighted in Fig. 8, KBNet fails to reconstruct the pole and leftmost street sign, NLSPN predicts the wrong shape for the middle street sign, and ENet, PENet, and NLSPN fails to reconstruct the top left building region. In Fig. 9, KBNet and ENet fail to reconstruct the tree, and NLSPN and PENet fail to predict a smooth surface for the bottom right building. In our predictions, we show that our method is able to address the (highlighted) error modes present in the various teachers and avoid distilling them (see Sec. 3 on main paper for details). This results in positive congruent training, where we

distill from a teacher only when it yields low reconstruction errors and avoid the error modes of individual teachers.

11 Limitations

As noted in our discussion (Sec. 5 from main paper), learning distilled regularities from teachers imposes several risks and limitations. The effectiveness of Monitored Distillation is lower bounded by training using the unsupervised loss, and upper bounded by the performance of teachers and their error modes. In particular, if all teachers yield high photometric reprojection errors on certain regions due to inaccurate depth values, the student model will have to rely on unsupervised losses rather than the distilled depth, which lower bounds our performance.

Our approach also depends on unsupervised photometric and structural losses that are limited by parallax. In stereo settings with insufficient baseline, or in monocular settings where there is insufficient movement between image frames, the photometric reprojection error would be limited in conveying information about the 3D scene layout for distant regions. Our approach is further limited by the identifiability of shape from the reprojection error, and relies on generic priors to resolve the aperture problem and blank-wall effects.

Lastly, our method struggles to explicitly handle non-Lambertian surfaces as we rely on photometric reprojection error for our ensembling method. However, we know from [24] that the domain coverage of specularities and translucency is sparse due to the sparsity of primary illuminants (rank of the reflectance tensor is deficient and typically small). So, explicitly modeling deviations from diffuse Lambertian reflection is likely to yield modest returns in accuracy of the reconstruction. Nevertheless, if desired, such surfaces can be accounted for by additionally incorporating sparse depth constraints (i.e. measuring error of each region through building a scaffold of the sparse depth consistency loss) in the selection process – however we note that this would impose additional computational costs on the selection process that scales with the number of teachers. For the proof of concept presented in this paper, we do not consider this.

Nonetheless, this is the first work to introduce Monitored Distillation for depth completion in the blind ensemble setting. Not only that, by leveraging Monitored Distillation, we are able to compress the student such that it can run in real-time, unlike the teachers. Our framework is general and we believe it can be formulated to be applied to a number of tasks e.g. unsupervised learning of geometry, outside of depth completion.